

# Confident Neural Network Regression with Bootstrapped Deep Ensembles

Laurens Sluijterman<sup>1</sup> Eric Cator<sup>1</sup> Tom Heskes<sup>2</sup>

## Abstract

With the rise of the popularity and usage of neural networks, trustworthy uncertainty estimation is becoming increasingly essential. In this paper we present a computationally cheap extension of Deep Ensembles for a regression setting called *Bootstrapped Deep Ensembles* that explicitly takes the effect of finite data into account using a modified version of the parametric bootstrap. We demonstrate through a simulation study that our method has comparable or better prediction intervals and superior confidence intervals compared to Deep Ensembles and other state-of-the-art methods. As an added bonus, our method is better capable of detecting overfitting than standard Deep Ensembles.

## 1. Introduction

Numerous different methods to obtain uncertainty estimates for neural networks exist (see [Abdar et al. \(2021\)](#) for an extensive overview). **Bayesian Neural Networks** ([MacKay, 1992](#); [Neal, 2012](#)) put a prior distribution over the weights of a network and use the posterior to obtain uncertainty estimates. The calculation of the posterior is often intractable. **Variational Inference** ([Hinton & Van Camp, 1993](#); [Jordan et al., 1999](#)) aims to solve this problem. **Monte-Carlo Dropout** ([Gal & Ghahramani, 2016](#); [Gal et al., 2017](#)) is a notable example of variational inference. Since dropout is already used in many networks as a regularization technique, it comes at no extra cost at training time. A downside is that the epistemic uncertainty is only influenced by the dropout rate. This makes it impossible to locally tune the uncertainty estimates to have the correct size ([Sluijterman et al., 2021](#)). **Quantile regression** ([Cannon, 2011](#); [Xu et al., 2017](#); [Clements et al., 2019](#); [Tagasovska & Lopez-Paz, 2019](#)) uses a pinball loss to output quantiles directly without the need of any distributional assumptions. Similarly, direct Prediction

Interval (PI) methods use a custom loss function that directly outputs PIs with the goal to capture the correct fraction of data points while being as narrow as possible ([Pearce et al., 2018](#)). Other methods are focussed more on detecting **out-of-distribution** (OoD) samples. These are input values that are very different from the training data. A typical approach is to keep track of the pre-activations, the output of the penultimate layer (or sometimes also other layers) times the weight matrix plus the bias vector, and use some distance measure to determine the level of difference of a new datapoint ([van Amersfoort et al., 2021](#); [Mukhoti et al., 2021](#); [Lee et al., 2018](#)). Similarly, ([Ren et al., 2019](#)) use likelihood ratios directly on the inputs to detect out-of-distribution samples. OoD detection methods do not aim for calibrated prediction or confidence intervals.

In this paper, we focus on ensembling methods and in particular on its currently most popular exponent, so-called Deep Ensembles (DE) ([Lakshminarayanan et al., 2017](#)). Ensembling methods train an ensemble of models and use the variance between predictions as a measure of uncertainty (see e.g., ([Heskes, 1997](#)) for an early example). Ensemble methods like DE accomplish two goals at once: the ensemble average reduces some of the variance and then provides a more accurate prediction than a random member, and the variance between the ensemble members can be used to estimate the uncertainty of the prediction. Deep Ensembles train an ensemble of  $M$  networks, each member getting the same data but in a different order and having a different initialisation. The architecture of the networks is similar to the mean variance estimation method by [Nix & Weigend \(1994\)](#). Each network outputs a mean and variance prediction for every input and is trained by minimizing the negative loglikelihood, assuming a normal distribution. We provide more details on this method in Section 3.1

Deep Ensembles have been shown to clearly outperform Variational Inference and Monte-Carlo Dropout ([Lakshminarayanan et al., 2017](#)) and are regarded the state of the art ([Wilson & Izmailov, 2020](#); [Ovadia et al., 2019](#); [Mukhoti et al., 2021](#); [Ashukha et al., 2020](#)). Different explanations for the success of Deep Ensembles have been given. [Wilson & Izmailov \(2020\)](#) relate the method to a form of Bayesian model averaging. They empirically demonstrate that DE is even able to better approximate the predictive distribution than some standard Bayesian approaches. Similarly,

<sup>1</sup>Department of Mathematics, Radboud University, Nijmegen, Netherlands <sup>2</sup>Institute for Computing and Information Sciences, Radboud University, Nijmegen, Netherlands. Correspondence to: Laurens Sluijterman <L.Sluijterman@math.ru.nl>.

Gustafsson et al. (2020) relate the method to sampling from an approximate posterior. Fort et al. (2019) explain the success via the loss landscape. They argue that the different models are able to explore different local minima, where a Bayesian approximation may only explore a single local minimum.

None of these interpretations fully explains why the obtained intervals would be properly calibrated. In fact, as we will also show in our experiments, by training each ensemble member on the same data, DE ignore a significant part of the epistemic uncertainty that is due to finite data. In Section 3 we introduce our method, *Bootstrapped Deep Ensembles*, an easy to implement extension of DE with comparable computational costs that does take this source of epistemic uncertainty into account.

Section 2 defines the uncertainty framework that we are considering. We precisely define the different types of uncertainty and intervals that we consider. In Section 4 we explain and give the results of our four experiments. We demonstrate the significance of the effect of finite data and show that incorporating this improves the confidence intervals significantly, which in turn can result in improved prediction intervals. Finally, Section 5 summarises the conclusions and gives possible avenues of future work.

## 2. Uncertainty Framework

We consider a frequentist regression setting in which a neural network is trained on a data set  $\mathcal{D}$  consisting of  $N$  i.i.d. observation pairs  $(\mathbf{x}, y)$ , with input  $\mathbf{x} \in \mathbb{R}^d$  and target  $y \in \mathbb{R}$ . We take the fixed-covariates perspective, meaning that we treat  $\mathbf{x}$  as being fixed and given and  $y$  as a random variable. The uncertainty due to finite data is therefore the uncertainty due to the randomness of the targets. To make this perspective explicit, we will use this terminology in the rest of the paper.

Given a new input  $\mathbf{x}^*$ , the neural network outputs a prediction  $\hat{f}(\mathbf{x})$  for the corresponding target  $y^*$ . The uncertainty about our prediction consists of two main components. Firstly, we are unsure about the true underlying function  $f(\mathbf{x})$ . This may be the result of a limited amount of, possibly noisy, data or due to randomness in our training procedure, such as random initialisation and batches. This is called *epistemic uncertainty*. Even if we were absolutely sure about  $f(\mathbf{x})$  we would still have the uncertainty in our prediction of  $y$  as a result of the noise, the *aleatoric uncertainty*. Where we may be able to reduce the epistemic uncertainty, e.g., by gathering more data or changing our optimization procedures, it is impossible to reduce the aleatoric uncertainty.

The certainty in our predictions can be expressed via a confidence and prediction interval. A confidence interval gives the region in which we expect our function value,  $f(\mathbf{x}^*)$ , to

fall. The prediction interval gives the region in which we expect a new observation  $y^*$  to fall. The confidence interval is determined only by the epistemic uncertainty while the prediction interval is also a function of the aleatoric uncertainty. Depending on the task, either the confidence or prediction interval may be of more interest.

The typical training process of a neural network is random both because of random initialisation and random batches. With  $U$  a random variable that describes this randomness, and  $\mathcal{Y}$  a random variable whose realisation is an entire set of targets corresponding to the fixed covariates in our data set  $\mathcal{D}$ , we can formally define a confidence interval as follows.

**Definition 2.1.** A  $(1 - \alpha) \cdot 100\%$  pointwise confidence interval for  $f$  is a random mapping,  $\text{CI}^{(\alpha)}(\mathcal{Y}, U, \cdot) : \mathbb{R}^d \rightarrow \mathcal{P}(\mathbb{R}) : \mathbf{x} \mapsto \text{CI}^{(\alpha)}(\mathcal{Y}, U, \mathbf{x})$ , such that

$$\mathbb{E}_{\mathcal{Y}, U} \left[ \mathbb{1}_{\{f(\mathbf{x}) \in \text{CI}^{(\alpha)}(\mathcal{Y}, U, \mathbf{x})\}} \right] = 1 - \alpha \quad \forall \mathbf{x}. \quad (1)$$

Here  $\mathcal{P}(\mathbb{R})$  is the power set of  $\mathbb{R}$ .

Analogously we have the following definition of a prediction interval:

**Definition 2.2.** A  $(1 - \alpha) \cdot 100\%$  pointwise prediction interval is a random mapping,  $\text{PI}^{(\alpha)}(\mathcal{Y}, U, \cdot) : \mathbb{R}^d \rightarrow \mathcal{P}(\mathbb{R}) : \mathbf{x} \mapsto \text{PI}^{(\alpha)}(\mathcal{Y}, U, \mathbf{x})$ , such that

$$\mathbb{E}_{\mathcal{Y}, U} \left[ \mathbb{E}_{Y|X=\mathbf{x}} \left[ \mathbb{1}_{\{Y \in \text{PI}^{(\alpha)}(\mathcal{Y}, U, \mathbf{x})\}} \right] \right] = 1 - \alpha \quad \forall \mathbf{x}. \quad (2)$$

By changing the equality in these definitions by a ' $\geq$ ' sign, we obtain a *conservative* confidence/prediction interval.

## 3. Bootstrapped Deep Ensembles

In this section we introduce our method Bootstrapped Deep Ensembles (BDE). We first review standard Deep Ensembles. The second subsection argues that Deep Ensembles can be improved by incorporating the uncertainty due to the random targets and explains how our method aims to do this. In Subsections 3.3 and 3.4 we discuss how to construct confidence and prediction intervals. Finally, in Subsection 3.5 we argue that our method is better able to detect overfitting than standard Deep Ensembles.

### 3.1. Deep Ensembles

The starting point is the same as Deep ensembles, which we review now.  $M$  networks are trained that each output a mean  $\hat{f}_i(\mathbf{x})$  and a variance  $\hat{\sigma}_i^2(\mathbf{x})$ . The networks are trained - on the same data, each with random initialisation and data ordering - by minimizing the negative loglikelihood of a normal distribution, which implies the following assumption.

**Assumption 3.1.** The targets,  $y$ , are the sum of a function value  $f(\mathbf{x})$  and normally distributed heteroscedastic noise:

$$y = f(\mathbf{x}) + \epsilon, \quad \text{with } \epsilon \sim \mathcal{N}(0, \sigma^2(\mathbf{x})).$$

The chosen predictive model is a Gaussian Mixture of the individual models. In this model the total mean and variance are defined as

$$\hat{f}_*(\mathbf{x}) = M^{-1} \sum_{i=1}^M \hat{f}_i(\mathbf{x}),$$

and

$$\hat{\sigma}_*^2(\mathbf{x}) = M^{-1} \sum_{i=1}^M \hat{f}_i(\mathbf{x})^2 - \hat{f}_*(\mathbf{x})^2 + \hat{\sigma}_i^2(\mathbf{x}). \quad (3)$$

This results in the prediction interval

$$\text{PI}_{\text{DE}} = \hat{f}_*(\mathbf{x}) \pm z_{\alpha/2} \sqrt{\hat{\sigma}_*^2(\mathbf{x})}.$$

For later comparison, we construct a confidence interval implied by DE by ignoring the aleatoric variance terms  $\hat{\sigma}_i^2(\mathbf{x})$  in Equation (3) to arrive at

$$\text{CI}_{\text{DE}} = \hat{f}_*(\mathbf{x}) \pm t_{\alpha/2}^{(M-1)} \sqrt{M^{-1} \sum_{i=1}^M \hat{f}_i(\mathbf{x})^2 - \hat{f}_*(\mathbf{x})^2},$$

where  $t_{\alpha/2}^{(M-1)}$  is the  $\alpha/2$  quantile of a  $t$  distribution with  $M-1$  degrees of freedom.

Our method uses the same setup and the same predictor  $\hat{f}_*(\mathbf{x})$ . The key difference is that we also include the epistemic uncertainty due to the random targets, resulting in different confidence and prediction intervals. As previously stated, we model a neural network as a random predictor with an error that decomposes in a part due to the training procedure and a part due to random targets. We formalize this in the following assumption.

**Assumption 3.2.** Let  $\hat{f}_i(\mathbf{x})$  be the prediction of an ensemble member trained on the same data set  $\mathcal{D}$ , but with a unique initialization and data ordering, and let  $f(\mathbf{x})$  be the true value, then

$$\hat{f}_i(\mathbf{x}) = f(\mathbf{x}) + \epsilon_d + \epsilon_{t,i}, \quad \text{with}$$

$$\epsilon_d \sim \mathcal{N}(0, \sigma_d^2(\mathbf{x})) \quad \text{and} \quad \epsilon_{t,i} \sim \mathcal{N}(0, \sigma_t^2(\mathbf{x})),$$

where all  $\epsilon$  are independent. We do not give  $\epsilon_d$  an index  $i$  to stress that this term is the same for all ensemble members.

From this point of view, the average of ensemble members trained on the same data,  $f_*(\mathbf{x})$ , has variance

$$\mathbb{V}(\hat{f}_*(\mathbf{x})) = \sigma_d^2(\mathbf{x}) + \frac{\sigma_t^2(\mathbf{x})}{M}. \quad (4)$$

Deep Ensembles are able to measure  $\sigma_t^2(\mathbf{x})$ , but fail to capture  $\sigma_d^2(\mathbf{x})$ . Since the  $M$  ensemble members are trained on the same data set, we can take the sample variance of these ensemble members as an estimate of the variance due to the random training:

$$\hat{\sigma}_t^2(\mathbf{x}) = \frac{1}{M-1} \sum_{i=1}^M \left( \hat{f}_i(\mathbf{x}) - \frac{1}{M} \sum_{i=1}^M \hat{f}_i(\mathbf{x}) \right)^2.$$

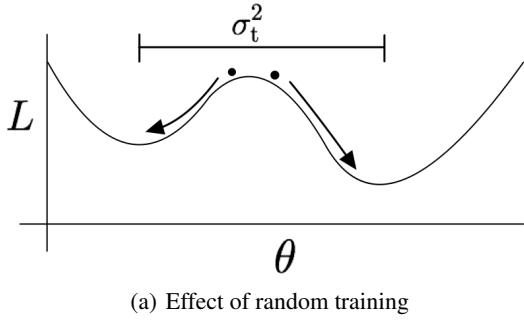
### 3.2. Incorporating the Missing Uncertainty

To estimate the missing  $\hat{\sigma}_d^2(\mathbf{x})$ , we propose to use an adapted version of the *parametric bootstrap* (Efron, 1982). For a standard parametric model, the parametric bootstrap consists of two steps. The model is trained on the data, after which  $B$  additional models are trained using new data, simulated from the first model. The variance of those extra models is then used to obtain the model uncertainty. Directly translating this to our setup has multiple problems. Training a new network on simulated targets would also capture the variance due to the training procedure. A solution could be to estimate the variance in Equation (4) directly by training  $B$  entire ensembles on simulated data sets, but this would be far to expensive. We therefore must find a way to train additional neural networks while eliminating training variability.

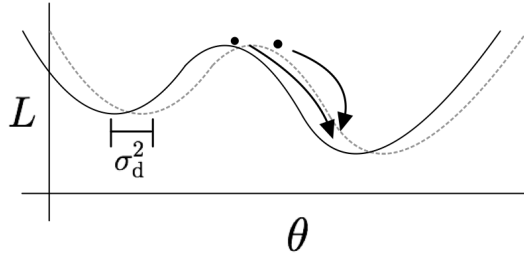
To explain how we do this, we examine the problem from a loss landscape perspective, as sketched in Figure 1. The random training causes the networks to end up in different local minima, while different targets cause the loss landscape to deform. Starting from a later point in the training cycle - as opposed to starting at initialisation - is much more likely to cause the retrained network to end up in the deformed version of the *same* local minimum, thus eliminating training variability. In order to estimate  $\sigma_d^2(\mathbf{x})$ , we therefore propose the following procedure. During the training of the original ensemble members, we save a copy of the state of the network after  $\lfloor N_e \cdot (1-r) \rfloor$  epochs, where  $N_e$  is total amount of training epochs and  $r \in [0, 1]$  is the retraining fraction. We then repeat the final  $r \cdot N_e$  epochs, starting from the saved state with new targets that are simulated from a  $\mathcal{N}(\hat{f}_i(\mathbf{x}), \hat{\sigma}_i^2(\mathbf{x}))$  distribution. We denote this retrained network with  $\hat{f}_i(\mathbf{x})$ .

We assume that this retraining captures solely the variance due to the random targets. A standard assumption of the parametric bootstrap is that the distributions of the difference of the first model and the true model, and the difference of the retrained model and the first model, are similar (Efron, 1982). In our case this assumption translates to:

**Assumption 3.3.** Let  $\hat{f}_i(\mathbf{x})$  denote the predictions of a retrained ensemble member. The difference between  $\hat{f}_i(\mathbf{x})$  and  $\hat{\hat{f}}_i(\mathbf{x})$  is normally distributed with zero mean and



(a) Effect of random training



(b) Effect of random targets

Figure 1. Figure (a) sketches the effect of the random training procedure. Through random initializations and random orderings of the data, different regions of the loss landscape get explored. We denote the variance that arises from this effect with  $\sigma_t^2$ . With finite training data, our loss landscape itself is subject to randomness. To estimate the resulting uncertainty, we apply the parametric bootstrap, resulting in new targets and a deformed loss landscape. To ensure we end up in the deformed version of the same local minimum, we repeat only a part of the training.

variance  $\sigma_d^2(\mathbf{x})$ :

$$\hat{f}_i(\mathbf{x}) = \hat{f}_i(\mathbf{x}) + \epsilon_i \quad \text{with} \quad \epsilon_i \sim \mathcal{N}(0, \sigma_d^2(\mathbf{x})).$$

As an estimate for  $\sigma_d^2(\mathbf{x})$  we therefore use

$$\hat{\sigma}_d^2(\mathbf{x}) = \frac{1}{M} \sum_{i=1}^M \left( \hat{f}_i(\mathbf{x}) - \hat{\hat{f}}_i(\mathbf{x}) \right)^2.$$

In a parametric model Assumptions 3.2 and 3.3 hold asymptotically, as we show in Appendix A. Therefore, they appear to be a logical first choice, also for finite data. We observed that these assumptions hold empirically in most of our simulations, as we demonstrate in Appendix A. The coverage values that we found, given in Section 4.3 also indicate that these assumptions are reasonable.

The entire method is summarised in Algorithm 1. With relatively little extra effort - we only need to train the equivalent of  $M(1 + r)$  networks, where  $r < 1$  - we are able to get uncertainty estimates that are better theoretically founded, as is explained in the next subsection, and empirically result in better confidence intervals, as is demonstrated in Section 4.3.

**Algorithm 1** Pseudo-code to obtain a confidence interval with Bootstrapped Deep Ensembles

```

1: Input:  $M$  - number of ensembles,  $N_e$  - number of
   training epochs,  $r$  - retrain fraction,  $(X, Y)$  - data set
2: for  $i = 1$  to  $M$  do
3:   Train ensemble member  $i$  on  $(X, Y)$  with random
      initialisation and data ordering to obtain  $\hat{f}_i(\mathbf{x})$  and
       $\hat{\sigma}_i^2(\mathbf{x})$ , while saving the model and optimizer state
      after  $N_e(1 - r)$  training epochs
4:   Simulate new targets:  $Y_{\text{new}} \sim \mathcal{N}(\hat{f}_i(X), \hat{\sigma}_i^2(X))$ .
5:   Repeat the final  $N_e r$  training epochs on  $(X, Y_{\text{new}})$ ,
      obtaining  $\hat{f}_i(\mathbf{x})$ .
6: end for
7:  $\hat{f}_*(\mathbf{x}) := \frac{1}{M} \sum_{i=1}^M \hat{f}_i(\mathbf{x})$ 
8:  $\hat{\sigma}_d^2(\mathbf{x}) := \frac{1}{M} \sum_{i=1}^M \left( \hat{f}_i(\mathbf{x}) - \hat{f}_*(\mathbf{x}) \right)^2$ 
9:  $\hat{\sigma}_t^2(\mathbf{x}) := \frac{1}{M-1} \sum_{i=1}^M \left( \hat{f}_*(\mathbf{x}) - \hat{f}_i(\mathbf{x}) \right)^2$ 
10: Calculate the  $1 - \alpha$  confidence interval:

```

$$\text{CI}^{(\alpha)}(\mathbf{x}) = \left[ \hat{f}_*(\mathbf{x}) \pm t_{\alpha/2}^{(M-1)} \sqrt{\hat{\sigma}_d^2(\mathbf{x}) + \frac{\hat{\sigma}_t^2(\mathbf{x})}{M}} \right]$$

### 3.3. Confidence Intervals

The following theorem states that, under Assumptions 3.2, and 3.3, the pointwise confidence interval given in Algorithm 1 is conservative.

**Theorem 3.4.** *Following the notation introduced above, let  $\hat{f}_*(\mathbf{x})$  be the average of the  $M$  ensemble members with predictions  $\hat{f}_i(\mathbf{x})$ . Let  $\hat{\hat{f}}_i(\mathbf{x})$  be the prediction of ensemble member  $i$  after a part of the training is repeated with newly simulated targets. Define  $\hat{\sigma}_t^2(\mathbf{x})$  and  $\hat{\sigma}_d^2(\mathbf{x})$  as in Algorithm 1. Under Assumptions 3.2 and 3.3, with probability at least  $(1 - \alpha) \cdot 100\%$ :*

$$f(\mathbf{x}) \in \hat{f}_*(\mathbf{x}) \pm t_{\alpha/2}^{(M-1)} \sqrt{\hat{\sigma}_d^2(\mathbf{x}) + \frac{\hat{\sigma}_t^2(\mathbf{x})}{M}}, \quad (5)$$

where  $t_{\alpha/2}^{(M-1)}$  is the critical value of a t-distribution with  $M - 1$  degrees of freedom.

**Proof** The result follows by evaluating

$$T^2 = \frac{(f(\mathbf{x}) - \hat{f}_*(\mathbf{x}))^2}{\hat{\sigma}_d^2(\mathbf{x}) + \frac{\hat{\sigma}_t^2(\mathbf{x})}{M}}.$$

In Appendix B we show that

$$\mathbb{P}(T^2 \geq F_{1-\alpha}(1, M-1)) \leq \alpha.$$

This result directly implies that

$$\mathbb{P}\left(t_{\alpha/2}^{(M-1)} \leq T \leq t_{1-\alpha/2}^{(M-1)}\right) \geq 1 - \alpha,$$

---

**Algorithm 2** Pseudo-code to obtain a prediction interval with Bootstrapped Deep Ensembles

---

```

1:  $\hat{\sigma}^2(\mathbf{x}) = \frac{1}{M} \sum_{i=1}^M \hat{\sigma}_i^2(\mathbf{x})$ 
2: for  $i = 1$  to  $N_t$  do
3:    $t_i \sim t(M - 1)$ 
4:    $\mu_i(\mathbf{x}) = \hat{f}_*(\mathbf{x}) + t_i \sqrt{\hat{\sigma}_d^2(\mathbf{x}) + \frac{\hat{\sigma}_t^2(\mathbf{x})}{M}}$ 
5:    $y_i \sim \mathcal{N}(\mu_i(\mathbf{x}), \hat{\sigma}^2(\mathbf{x}))$ 
6:   Take the  $(1 - \alpha/2)$  and  $\alpha/2$  empirical quantiles of all  $y_i$  as the bounds of the prediction interval
7: end for

```

---

such that with probability of at least  $(1 - \alpha) \cdot 100\%$

$$f(\mathbf{x}) \in \hat{f}_*(\mathbf{x}) \pm t_{\alpha/2}^{(M-1)} \sqrt{\hat{\sigma}_d^2(\mathbf{x}) + \frac{\hat{\sigma}_t^2(\mathbf{x})}{M}}. \quad \square$$

We are now able to construct conservative pointwise confidence intervals for  $f(\mathbf{x})$  using any number of ensemble networks. The precise coverage depends on how well the assumptions hold in practice.

### 3.4. Prediction Intervals

The confidence interval from Theorem 3.4 can be easily extended to a prediction interval. The prediction interval combines the aleatoric uncertainty, governed by a normal distribution with variance  $\sigma^2(\mathbf{x})$ , with the epistemic uncertainty, a scaled student distribution with  $M - 1$  degrees of freedom. Algorithm 2 describes a Monte-Carlo sampling procedure to quickly estimate empirical quantiles of the resulting distribution.

### 3.5. Detecting Overfitting

An added bonus of our method is the possibility to detect overfitting. Suppose we are in a situation where the networks are overfitting to the point where the noise is being fit. The ensemble members of standard DE, that are trained on the exact same targets, will tend to provide the same predictions when overfitting on the targets, yielding very small confidence intervals. The retrained ensemble members of Bootstrapped DE, on the other hand, are trained on different targets and hence will tend to provide quite different predictions from their original counterparts, leading to relatively large confidence intervals. With extreme overfitting, to the point that  $\hat{\sigma}^2(\mathbf{x})$  gets close to zero, this advantage of bootstrapped DE over DE will vanish and both methods will fail to detect overfitting.

## 4. Experimental Results

In this section we examine the quality of the confidence and prediction intervals. In Subsection 4.1 we motivate why and how we simulated data for our experiments. We explain

---

**Algorithm 3** Pseudo-code to simulate data

---

```

1: Train a random forest on  $\mathcal{D}$  and use this forest as the true function  $f(\mathbf{x})$ 
2: Calculate the residuals,  $(Y - f(X))$ 
3: Train a second random forest on the squared residuals and use this function for the true variance  $\sigma^2(\mathbf{x})$ 
4: Simulate new targets:  $y_{\text{new}} \sim \mathcal{N}(f(\mathbf{x}), \sigma^2(\mathbf{x}))$ 
5: Return:  $\mathcal{D}_{\text{new}} = (X, Y_{\text{new}})$ 

```

---

both our experimental setup and our training procedures of our four experiments in Subsection 4.2 and give the results in Subsection 4.3.

### 4.1. Simulating Data

Since we want to compare confidence intervals, it is necessary to know the true function values. A simple toy experiment, however, may not be representative for a real-world scenario. To overcome this we set up simulations based on the benchmark data sets used in Hernández-Lobato & Adams (2015) using Algorithm 3. We take a data set, for instance Boston Housing, and train a random forest to predict  $y$  given  $\mathbf{x}$ . We use this model as the true function  $f(\mathbf{x})$ . We then train a second forest to predict the residuals squared  $(y - f(\mathbf{x}))^2$  and use this forest as the true variance  $\sigma^2(\mathbf{x})$ . Using this  $f(\mathbf{x})$  and  $\sigma^2(\mathbf{x})$  we simulate new data points from a  $\mathcal{N}(f(\mathbf{x}), \sigma^2(\mathbf{x}))$  distribution.

### 4.2. Experimental Setup

#### 4.2.1. Experiment 1: Simulations Based on Benchmark Data Sets

We first evaluate the quality of the prediction and confidence intervals. We compare our prediction intervals to Deep Ensembles, Concrete Dropout (CD) (Gal et al., 2017), and Quality-Driven Ensembles (QDE) (Pearce et al., 2018). The confidence intervals are compared to Deep Ensembles, the Naive Bootstrap (NB) (Efron, 1982; Heskes, 1997), and Concrete Dropout. A popular method to quantify the quality of a prediction interval or confidence interval is to look at the empirical coverage of the intervals on a previously unseen part of a real-world data set (Khosravi et al., 2011; Pearce et al., 2020; Su et al., 2018). However, it has been argued that it is not sufficient to evaluate the quality of prediction and confidence intervals in this manner on a test set. This only checks the overall coverage, which is relatively easy to tune, and not the quality of the pointwise confidence intervals (Sluijterman et al., 2021). The proposed alternative is to use simulated data and calculate the coverage per  $\mathbf{x}$  over a large number of simulations. This gives rise to the

*Table 1.* Results of the comparison of our method Bootstrapped Deep Ensembles (BDE) to Deep Ensembles (DE), the Naive Bootstrap (NB), Concrete Dropout (CD) and Quality Driven Ensembles (QDE). A total of 100 simulated data sets were used to calculate the metrics. On each new data set, new ensembles were trained, and new confidence and prediction intervals were constructed. Brier-CI80 denotes the Brier score of the CICF (Equation (6)) of an 80% confidence interval. Brier-PI80 denotes the equivalent quantity for the PICF (Equation (8)). We observe comparable Brier scores for most prediction intervals and significantly lower scores for all but two confidence intervals. The confidence intervals of BDE are wider but this is justified by the superior coverage. BDE and DE have identical RMSE since they use the same predictor. The RMSE value of CD was in general extremely similar. NB had a notably larger RMSE (often around 20%). This is to be expected since each ensemble member is effectively being trained on less data due to the resampling. All RMSE values, as well as a further comparison to Deep Ensembles, including training without regularisation, with a different base simulation model, and differently distributed noise, can be found in Appendix C.

SIMULATION	BRIER-CI80 ↓	BRIER-PI80 ↓	WIDTH CI80	WIDTH PI80
	BDE / DE / NB / CD $\times 10^{-2}$	BDE / DE / QDE / CD $\times 10^{-2}$	BDE / DE / NB / CD	BDE / DE / QDE / CD
BOSTON	<b>7.8</b> / 11 / 18 / <b>7.8</b>	2.4 / 3.5 / 3.1 / <b>1.5</b>	3.4 / 3.0 / 4.0 / 3.7	7.6 / 8.6 / 14.8 / 8.6
CONCRETE	<b>2.6</b> / 8.2 / 33 / 15	<b>0.80</b> / 1.5 / 1.5 / 2.6	8.7 / 6.4 / 7.9 / 6.0	18.3 / 17.0 / 32.1 / 16.2
ENERGY	4.0 / 6.7 / 37 / <b>1.5</b>	0.80 / 1.3 / 1.7 / <b>0.59</b>	2.3 / 1.8 / 2.0 / 2.1	4.5 / 5.2 / 13.3 / 4.4
KIN8NM	0.78 / <b>0.63</b> / 62 / 51	<b>0.13</b> / 0.25 / 0.93 / 3.1	0.17 / 0.14 / 0.12 / 0.024	0.53 / 0.52 / 0.69 / 0.44
NAVAL	<b>2.1</b> / 3.6 / 59 / 30	0.24 / 0.19 / 1.1 / <b>0.11</b>	(2.2 / 1.4 / 1.2 / 0.7) <sup>1</sup>	0.03 / 0.03 / 0.03 / 0.03
POWER-PLANT	<b>8.5</b> / 12 / 33 / 36	0.078 / <b>0.066</b> / 2.3 / 0.21	3.1 / 2.2 / 2.8 / 0.78	10.7 / 10.4 / 19.2 / 9.9
YACHT	<b>11</b> / 14 / 22 / <b>11</b>	<b>2.8</b> / 4.3 / 12 / 3.7	2.7 / 2.4 / 3.5 / 7.3	2.7 / 2.4 / 3.5 / 7.3
WINE	<b>0.89</b> / 2.6 / 8.6 / 26	0.95 / 1.5 / <b>0.80</b> / 6.2	0.50 / 0.45 / 0.68 / 0.27	1.4 / 1.4 / 2.1 / 1.1

<sup>1</sup>  $\times 10^{-3}$ 

Confidence Interval Coverage Fraction (CICF):

$$\text{CICF}(\mathbf{x}) := \frac{1}{n_{\text{sim}}} \sum_{j=1}^{n_{\text{sim}}} \mathbb{1}_{f(\mathbf{x}) \in [LC^{(j)}(\mathbf{x}), RC^{(j)}(\mathbf{x})]}, \quad (6)$$

where  $n_{\text{sim}}$  is the number of simulations,  $f(\mathbf{x})$  is the true function value, and  $LC^{(j)}(\mathbf{x}), RC^{(j)}(\mathbf{x})$  are the lower and upper limit of the CI of  $f(\mathbf{x})$  in simulation  $j$ . If we have a CI with the correct coverage in the sense of Definition 2.1, the CICF( $\mathbf{x}$ ) should be close to  $1 - \alpha$  for each value of  $\mathbf{x}$ . The following Brier score – with a perfect score of 0 meaning a CICF of  $1 - \alpha$  for each individual value of  $\mathbf{x}$  – accurately captures this:

$$\text{BS} = \frac{1}{n_{\text{test}}} \sum_{i=1}^{n_{\text{test}}} (\text{CICF}(\mathbf{x}_i) - (1 - \alpha))^2. \quad (7)$$

Evaluating the quality of the prediction interval is done similarly. We first define the Prediction Interval Coverage Probability:

$$\text{PICF}(\mathbf{x}) := \frac{1}{n_{\text{sim}}} \sum_{j=1}^{n_{\text{sim}}} \mathbb{P} \left( y \in [L^{(j)}(\mathbf{x}), R^{(j)}(\mathbf{x})] \right), \quad (8)$$

and then compute the resulting Brier scores. Apart from the Brier scores we also report the average widths of the intervals. In case of a comparable Brier score, we favor the method with smaller intervals. In Appendix C we also test the effect of differently distributed noise, a different simulation method, and different retraining fractions.

#### 4.2.2. Experiment 2: Relative Effect of Random Targets

As argued above, a neural network can be seen as a random predictor. This randomness is partially a consequence of the random training procedure and initialisation, which is captured well by Deep Ensembles. However, especially for small training sets, the random targets are also a significant source of variance in the predictor. We evaluated how large this effect is. We set up a simulation based on the large Protein-tertiary-structure data set. We trained 50 networks with random targets and 50 networks with fixed targets, all with random initialization and random batch orderings, on an increasing number of data points  $N$ . The random targets were simulated using Algorithm 3. We subsequently examined the average variance of the networks with fixed and random targets on 5000 previously unseen test points, denoted by  $\sigma_{\text{fixed}}^2$  and  $\sigma_{\text{random}}^2$  respectively. We consider  $\sigma_{\text{fixed}}^2$  an estimate of  $\sigma_t^2$  and  $\sigma_{\text{random}}^2 - \sigma_{\text{fixed}}^2$  an estimate of  $\sigma_d^2$ . Plotting these quantities for increasing  $N$  gives insight into the relative importance of the effect of random targets.

#### 4.2.3. Experiment 3: Variance Decomposition

We want to test how well Bootstrapped DE are indeed able to capture the variance due to the randomness of the targets. We therefore trained a Bootstrapped Deep Ensemble with  $M = 50$  and  $r = 30\%$  on a single data set generated with Algorithm 3. We also trained 50 networks using newly simulated targets for each network. We expect the predictions of those second 50 networks to have a variance

of  $\sigma_d^2(\mathbf{x}) + \sigma_t^2(\mathbf{x})$ , and the predictions of the first 50 networks (before retraining) to have a variance of  $\sigma_t^2(\mathbf{x})$ . If our assumptions are correct, our estimate  $\hat{\sigma}_d^2(\mathbf{x})$  should be roughly the difference between  $\sigma_d^2(\mathbf{x}) + \sigma_t^2(\mathbf{x})$  and  $\sigma_t^2(\mathbf{x})$ .

#### 4.2.4. Experiment 4: Detecting overfitting

We argued that Bootstrapped DE have a better chance to detect overfitting than standard DE. We give a motivating example by comparing BDE and DE in a scenario in which we know that the network will overfit: a complex network with only 7 data points and no regularisation. The targets were simulated from a  $\mathcal{N}(0, 0.2^2)$  distribution. Each ensemble member had three hidden layers containing 400, 200, and 100 hidden layers and was trained for 80 epochs.

#### 4.2.5. Training Procedure

For our first three experiments we used neural networks with three hidden layers having 40, 30, and 20 units respectively, ReLU activation functions in these hidden layers, and a linear activation function in the final layer. To ensure positivity of  $\hat{\sigma}$  we used an exponential transformation and added a minimum value of 1e-3 for numerical stability for the ensemble networks. Each network was trained for 80 epochs with a batchsize of 32 using the ADAM optimizer. This setup is very similar to those used in (Gal & Ghahramani, 2016) and (Hernández-Lobato & Adams, 2015) with the exception that we use more than one hidden layer. We do this because we observed a much larger bias when using only one layer. We set  $r = 30\%$  and  $M = 5$ . We used  $l_2$  regularisation with a standard constant of  $1/(\#\text{Training Samples})$ . The networks used for the Concrete Dropout and Quality Driven Ensembles methods were trained for 240 epochs each since we found that these networks needed longer to converge. All training data was standardized to have zero mean and unit variance before training. All testing was done on the original scales. The code has been made available at [https://github.com/LaurensSluyterman/Bootstrapped\\_Deep\\_Ensembles/tree/master](https://github.com/LaurensSluyterman/Bootstrapped_Deep_Ensembles/tree/master).

### 4.3. Results

#### 4.3.1. Experiment 1

The results are given in Table 1. Additional results can be found in Appendix C. We can see that the quality of our confidence intervals is considerably better than the confidence intervals obtained by other methods for most simulations. For example, in the simulation based on the Concrete data set the Brier score for the CICF range from 0.026 (BDE) to 0.33 (NB). To illustrate the significance of these differences we visualised the individual CICF scores as a violin plot in Figure 2. We note that for most values of  $\mathbf{x}$  the confidence intervals created with our method have the correct size. We

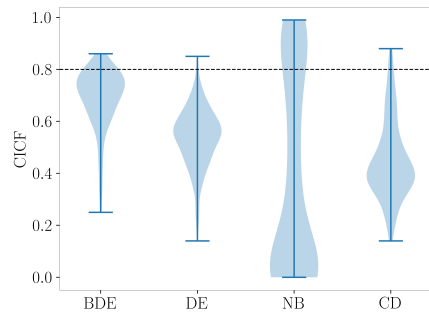


Figure 2. Violin plot of the individual  $\text{CICF}(\mathbf{x})$  values for 80% CIs, calculated on the test set of the *Concrete* simulation. Each  $\text{CICF}$  value was obtained using 100 simulations. Violin plots of all other simulations, including for the  $\text{PICF}$  values, can be found in Appendix C. Note that perfect coverage would correspond to a delta-peak at  $1 - \alpha$ . It can be seen that the confidence intervals for Deep Ensembles (DE) tend to be too optimistic, those for Concrete Dropout (CD) are often far too optimistic, and those for the Naive Bootstrap (NB) are all over the place.

observe that the confidence intervals for some points are still too small. In Figure 3 we can see that this is caused by a bias – defined as the difference between  $\hat{f}_*(\mathbf{x})$  and  $f(\mathbf{x})$  averaged over all simulations – in which case Assumption 3.2 does not hold. The points with a high bias have a worse CICF score. We note that Deep Ensembles have the same problem and that even on points with high bias our method has better CICF values. Another interesting observation is

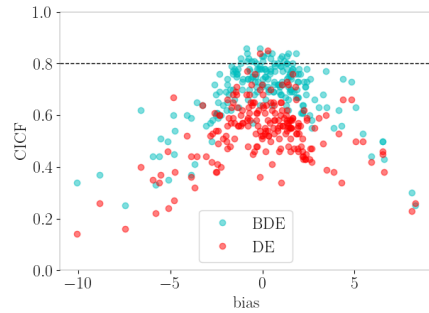


Figure 3. Illustration that both ensembling methods fail in case of a high bias. This figure was made on a simulation of 100 runs on the *Concrete* simulation. In each run an 80% confidence interval was made using both Bootstrapped Deep Ensembles (BDE) and Deep Ensembles (DE).

that the  $\text{PICF}$  values are higher in each experiment. This suggests that making a calibrated confidence interval is inherently more difficult than creating a prediction interval. It also demonstrates that in order to assess the quality of a confidence interval, it is not sufficient to only evaluate the predictive uncertainty.

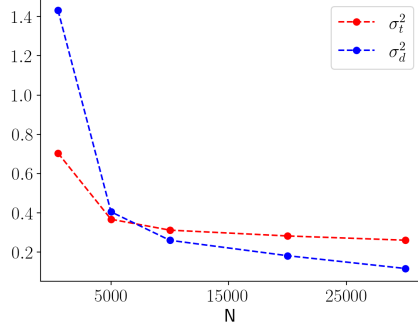


Figure 4. The effect of random targets and random training on the total variance of the predictor  $\hat{f}(\mathbf{x})$ , trained on the simulated *Protein* data set. The variance due to random training,  $\sigma_t^2$ , is obtained by examining the variance of 50 networks trained on the same data. Another 50 networks are trained on 50 different data sets, each with new targets. The variance of the second group is an estimate of  $\sigma_t^2 + \sigma_d^2$ . For small  $N$  the effect of random targets is dominant, and even for quite large  $N$ , it is still significant.

#### 4.3.2. Experiment 2

We can explain the undersized confidence intervals of Deep Ensembles with the second experiment. Figure 4 shows that with less than 5000 data points the random targets are the dominant source of variance and even with a lot of training data, the effect of random targets is still significant.

#### 4.3.3. Experiment 3

Table 2 shows that our separate estimates for the variances due to random targets and due to random training sum correctly - within approximately 10% - to the variance when training with random targets.

Table 2. The quality of the average estimate for  $\sigma_d^2(\mathbf{x})$  on 4 different simulated data sets. The first column gives the ground truth of  $\sigma_d^2 + \sigma_t^2$ , obtained by training with random targets. The sum of the estimates for  $\sigma_t^2$  (column three) and  $\sigma_d^2$  (column 4) match the ground truth within roughly 10%.

SIMULATION	$\sigma_d^2 + \sigma_t^2$	$\hat{\sigma}_t^2$	$\hat{\sigma}_d^2$	$\hat{\sigma}_t^2 + \hat{\sigma}_d^2$
BOSTON	2.44	1.52	0.91	2.43
CONCRETE	13.03	6.45	6.02	12.47
ENERGY	0.92	0.50	0.45	0.95
KIN8NM	2.7E-3	1.7E-3	1.6E-3	3.3E-3

#### 4.3.4. Experiment 4: Overfitting

Figure 5 illustrates that BDE is better able to detect overfitting. The confidence intervals of our method increase at the location of the data points, indicating overfitting, whereas those of DE almost vanish.

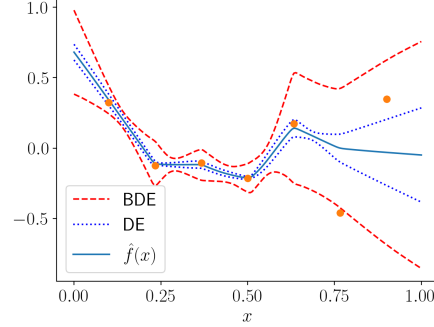


Figure 5. The 90% confidence intervals of Bootstrapped Deep Ensembles (BDE) and Deep Ensembles (DE). The original ensemble members were trained long enough to overfit on the data. DE are unable to detect this since all ensemble members behave roughly the same. The variance of the networks after retraining on new targets, however, is much larger each network will overfit on *different* targets. BDE are therefore better able to detect overfitting.

## 5. Conclusion

In this paper we presented our uncertainty estimation method Bootstrapped Deep Ensembles. The BDE confidence intervals have a much better coverage and are better able to detect overfitting than those obtained with standard DE or other popular methods, at a price of just 30% more training time.

BDE improves upon DE because it incorporates the epistemic uncertainty due to the randomness of the training targets, where DE only captures the randomness of the optimization procedure. Our simulations show that the randomness of the training targets is substantial, even for larger data sets. Where based on asymptotic statistical theory one would expect this variance to be inversely proportional to the number of data points, we observed a slower decay, closer to  $\frac{1}{\sqrt{N}}$ . It would be interesting to study the (asymptotic) behavior of these two components in more detail, also to be able to judge when one can indeed be neglected compared to the other.

In regions with relatively little data, confidence intervals tend to get larger. In general, however, we would like to discourage the use of confidence intervals for out-of-distribution detection: confidence intervals may get wider for quite different reasons, in particular when we allow for heteroscedastic noise, and, perhaps more importantly, they simply cannot be trusted in regions with little training data, since the underlying assumptions on which they are based are doomed to be violated. A more promising avenue for future work is to combine our method with an orthogonal approach, specifically for OoD detection (such as Ren et al. (2019)).

## References

- Abdar, M., Pourpanah, F., Hussain, S., Rezazadegan, D., Liu, L., Ghavamzadeh, M., Fieguth, P., Cao, X., Khosravi, A., Acharya, U. R., et al. A review of uncertainty quantification in deep learning: Techniques, applications and challenges. *Information Fusion*, 2021.
- Ashukha, A., Lyzhov, A., Molchanov, D., and Vetrov, D. Pitfalls of in-domain uncertainty estimation and ensembling in deep learning. *arXiv preprint arXiv:2002.06470*, 2020.
- Cannon, A. J. Quantile regression neural networks: Implementation in r and application to precipitation downscaling. *Computers & Geosciences*, 37(9):1277–1284, 2011.
- Clements, W. R., Robaglia, B.-M., Van Delft, B., Slaoui, R. B., and Toth, S. Estimating risk and uncertainty in deep reinforcement learning. *arXiv preprint arXiv:1905.09638*, 2019.
- Efron, B. *The Jackknife, the Bootstrap and other Resampling Plans*. SIAM, 1982.
- Fort, S., Hu, H., and Lakshminarayanan, B. Deep ensembles: A loss landscape perspective. *arXiv preprint arXiv:1912.02757*, 2019.
- Gal, Y. and Ghahramani, Z. Dropout as a Bayesian approximation: Representing model uncertainty in deep learning. In *International Conference on Machine Learning*, pp. 1050–1059, 2016.
- Gal, Y., Hron, J., and Kendall, A. Concrete dropout. *Advances in Neural Information Processing Systems*, 30, 2017.
- Gustafsson, F. K., Danelljan, M., and Schon, T. B. Evaluating scalable Bayesian deep learning methods for robust computer vision. In *Proceedings of the IEEE/CVF Conference on Computer Vision and Pattern Recognition Workshops*, pp. 318–319, 2020.
- Hernández-Lobato, J. M. and Adams, R. Probabilistic back-propagation for scalable learning of Bayesian neural networks. In *International Conference on Machine Learning*, pp. 1861–1869, 2015.
- Heskes, T. Practical confidence and prediction intervals. In *Advances in Neural Information Processing Systems*, pp. 176–182, 1997.
- Hinton, G. E. and Van Camp, D. Keeping the neural networks simple by minimizing the description length of the weights. In *Proceedings of the sixth annual conference on Computational Learning Theory*, pp. 5–13, 1993.
- Jordan, M. I., Ghahramani, Z., Jaakkola, T. S., and Saul, L. K. An introduction to variational methods for graphical models. *Machine Learning*, 37(2):183–233, 1999.
- Khosravi, A., Nahavandi, S., Creighton, D., and Atiya, A. F. Comprehensive review of neural network-based prediction intervals and new advances. *IEEE Transactions on Neural Networks*, 22(9):1341–1356, 2011.
- Lakshminarayanan, B., Pritzel, A., and Blundell, C. Simple and scalable predictive uncertainty estimation using deep ensembles. In *Advances in Neural Information Processing Systems*, pp. 6402–6413, 2017.
- Lee, K., Lee, K., Lee, H., and Shin, J. A simple unified framework for detecting out-of-distribution samples and adversarial attacks. In *Advances in Neural Information Processing Systems*, 2018.
- MacKay, D. J. A practical Bayesian framework for back-propagation networks. *Neural Computation*, 4(3):448–472, 1992.
- Mukhoti, J., Kirsch, A., van Amersfoort, J., Torr, P. H., and Gal, Y. Deterministic neural networks with appropriate inductive biases capture epistemic and aleatoric uncertainty. *arXiv preprint arXiv:2102.11582*, 2021.
- Neal, R. M. *Bayesian Learning for Neural Networks*, volume 118. Springer Science & Business Media, 2012.
- Nix, D. A. and Weigend, A. S. Estimating the mean and variance of the target probability distribution. In *Proceedings of 1994 IEEE International Conference on Neural Networks (ICNN'94)*, volume 1, pp. 55–60. IEEE, 1994.
- Ovadia, Y., Fertig, E., Ren, J., Nado, Z., Sculley, D., Nowozin, S., Dillon, J., Lakshminarayanan, B., and Snoek, J. Can you trust your model’s uncertainty? Evaluating predictive uncertainty under dataset shift. *Advances in Neural Information Processing Systems*, 32:13991–14002, 2019.
- Pearce, T., Brintrup, A., Zaki, M., and Neely, A. High-quality prediction intervals for deep learning: A distribution-free, ensembled approach. In *International Conference on Machine Learning*, pp. 4075–4084, 2018.
- Pearce, T., Leibfried, F., and Brintrup, A. Uncertainty in neural networks: Approximately Bayesian ensembling. In *International Conference on Artificial Intelligence and Statistics*, pp. 234–244. PMLR, 2020.
- Ren, J., Liu, P. J., Fertig, E., Snoek, J., Poplin, R., Depristo, M., Dillon, J., and Lakshminarayanan, B. Likelihood ratios for out-of-distribution detection. *Advances in Neural Information Processing Systems*, 32:14707–14718, 2019.

Seber, G. and Wild, C. *Nonlinear Regression*. Wiley, 2003.

Sluijterman, L., Cator, E., and Heskes, T. How to evaluate uncertainty estimates in machine learning for regression? *arXiv preprint arXiv:2106.03395*, 2021.

Su, D., Ting, Y. Y., and Ansel, J. Tight prediction intervals using expanded interval minimization. *arXiv preprint arXiv:1806.11222*, 2018.

Tagasovska, N. and Lopez-Paz, D. Single-model uncertainties for deep learning. In *Advances in Neural Information Processing Systems*, pp. 6417–6428, 2019.

van Amersfoort, J., Smith, L., Jesson, A., Key, O., and Gal, Y. Improving deterministic uncertainty estimation in deep learning for classification and regression. *arXiv preprint arXiv:2102.11409*, 2021.

Van der Vaart, A. W. *Asymptotic Statistics*, volume 3. Cambridge University Press, 2000.

Wilson, A. G. and Izmailov, P. Bayesian deep learning and a probabilistic perspective of generalization. *arXiv preprint arXiv:2002.08791*, 2020.

Xu, Q., Deng, K., Jiang, C., Sun, F., and Huang, X. Composite quantile regression neural network with applications. *Expert Systems with Applications*, 76:129–139, 2017.

---

## Confident Neural Network Regression with Bootstrapped Deep Ensembles: Appendix

---

This appendix consists of three parts. In Appendix A we motivate the assumptions on which Bootstrapped Deep Ensembles rely. In Appendix B, we complete the proof of Theorem 3.4 that uses these assumptions to construct a confidence interval. Finally, we provide additional experimentation in Appendix C.

### A. Motivation of Assumptions

Our method makes use of Assumptions 3.1, 3.2, and 3.3. We will first provide a theoretical motivation of these assumptions and then provide some additional empirical support.

#### A.1. Theoretical Motivation of Assumptions

Assumption 3.1 is a common modeling assumption that may or may not hold depending on the data. The second assumption claims that the output of the neural network is normally distributed. In a deterministic parametric model without regularisation we can demonstrate that this assumption holds asymptotically. In this case there is no variance due to training and we need to show - 1 - that the output of the model is normally distributed and - 2 - that if we train the model again on simulated targets, that the output will still be normally distributed with roughly equal variance.

Let  $\theta$  be the parameters that parametrize our network. Let  $p_\theta(\mathcal{D})$  be the likelihood of the data given  $\theta$ . Our setup corresponds to finding the  $\theta$  that maximizes  $p_\theta(\mathcal{D})$ :

$$\hat{\theta} = \arg \max_{\theta} p_\theta(\mathcal{D}),$$

and subsequently finding  $\hat{\hat{\theta}}$  that maximises  $p_\theta(\mathcal{D}_{\text{new}})$ :

$$\hat{\hat{\theta}} = \arg \max_{\theta} p_\theta(\mathcal{D}_{\text{new}}),$$

Furthermore, we define

$$I(\theta_0) := \text{Cov}_{\theta_0} \left. \frac{\partial}{\partial \theta} \log(p_\theta(\mathbf{x}_1, y_1)) \right|_{\theta_0}. \quad (9)$$

Under certain consistency and regularity conditions it is possible to show that

$$\sqrt{n}(\hat{\theta} - \theta_0) \rightarrow \mathcal{N}(0, I(\theta_0)^{-1}),$$

and

$$\sqrt{n}(\hat{\hat{\theta}} - \hat{\theta}) \rightarrow \mathcal{N}(0, I(\hat{\theta})^{-1}).$$

For a proof and clarification of the assumed consistency and regularity see [Van der Vaart \(2000\)](#) or [Seber & Wild \(2003\)](#).

With  $\hat{f}_i$  and  $\hat{\hat{f}}_i$  we denote the output of the mean prediction of an ensemble member before and after repeating part of the training. The delta method gives the variance of  $\hat{f}_i$  and  $\hat{\hat{f}}_i$ :

$$\mathbb{V}(\hat{f}_{\hat{\theta}}(\mathbf{x})) = \left. \frac{\partial}{\partial \theta} f_\theta(\mathbf{x}) \right|_{\theta_0} \mathbb{V}(\hat{\theta}) \left( \left. \frac{\partial}{\partial \theta} f_\theta(\mathbf{x}) \right|_{\theta_0} \right)^T,$$

and

$$\mathbb{V}(\hat{\hat{f}}_{\hat{\theta}}(\mathbf{x})) = \left. \frac{\partial}{\partial \theta} f_\theta(\mathbf{x}) \right|_{\hat{\theta}} \mathbb{V}(\hat{\hat{\theta}}) \left( \left. \frac{\partial}{\partial \theta} f_\theta(\mathbf{x}) \right|_{\hat{\theta}} \right)^T.$$

Under the assumed consistency,  $\hat{\theta}$  and  $\hat{\hat{\theta}}$  will be close and thus  $\frac{\partial}{\partial \theta} f_\theta(\mathbf{x})|_{\hat{\theta}}$  will be close to  $\frac{\partial}{\partial \theta} f_\theta(\mathbf{x})|_{\hat{\hat{\theta}}}$ . By the same consistency,  $I(\theta_0)$  and  $I(\hat{\theta})$  will be close.

## A.2. Empirical Assessment of Assumptions

During the Boston Housing part of experiment 1, we kept track of all the predictions of the first ensemble member before and after retraining in each of the 100 simulations. Figure 6 shows two typical scenarios. For most values of  $\mathbf{x}$  we found that the errors are indeed normally distributed and that the variance of  $\hat{f}_i(\mathbf{x}) - f(\mathbf{x})$  is slightly larger than the variance of  $\hat{\hat{f}}_i(\mathbf{x}) - \hat{f}_i(\mathbf{x})$ . This is expected, since the former also has variance due to the randomness of the training. We also see, however, that for some values of  $\mathbf{x}$  we get a large bias term, violating Assumption 3.2. In the main text we demonstrate that the method fails in this scenario.

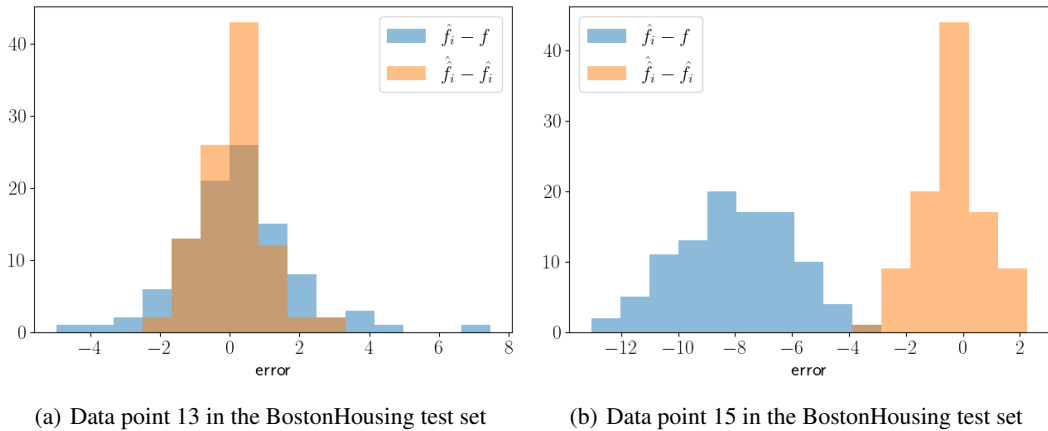


Figure 6. Empirical example of Assumptions 3.2 and 3.3. Each histogram is made by evaluating  $\hat{f}_i(\mathbf{x}) - f(\mathbf{x})$  and  $\hat{\hat{f}}_i(\mathbf{x}) - \hat{f}_i(\mathbf{x})$  for a single value of  $\mathbf{x}$  on 100 simulated data sets. In (a) we see that the assumptions appear to hold. We have normally distributed errors with a slightly smaller variance after retraining. This should be the case since the aim of the retraining is to only capture the variance due to the random targets and not the random training. In (b), however, we see that for some values of  $\mathbf{x}$ , a large bias can occur.

## B. Proof Theorem 3.4

**Theorem 3.4.** *Following the notation introduced above, let  $\hat{f}_*(\mathbf{x})$  be the average of the  $M$  ensemble members with predictions  $\hat{f}_i(\mathbf{x})$ . Let  $\hat{\hat{f}}_i(\mathbf{x})$  be the prediction of ensemble member  $i$  after a part of the training is repeated with newly simulated targets. Define  $\hat{\sigma}_t^2(\mathbf{x})$  and  $\hat{\sigma}_d^2(\mathbf{x})$  as in Algorithm 1. Under Assumptions 3.2 and 3.3, with probability at least  $(1 - \alpha) \cdot 100\%$ :*

$$f(\mathbf{x}) \in \hat{f}_*(\mathbf{x}) \pm t_{\alpha/2}^{(M-1)} \sqrt{\hat{\sigma}_d^2(\mathbf{x}) + \frac{\hat{\sigma}_t^2(\mathbf{x})}{M}}, \quad (5)$$

where  $t_{\alpha/2}^{(M-1)}$  is the critical value of a t-distribution with  $M - 1$  degrees of freedom.

**Proof** The result follows by evaluating

$$T^2 = \frac{(f(\mathbf{x}) - \hat{f}_*(\mathbf{x}))^2}{\hat{\sigma}_d^2(\mathbf{x}) + \frac{\hat{\sigma}_t^2(\mathbf{x})}{M}}. \quad (10)$$

We recall that our estimates for  $\sigma_t^2(\mathbf{x})$  and  $\sigma_d^2(\mathbf{x})$  are given by:

$$\hat{\sigma}_t^2(\mathbf{x}) = \frac{1}{M-1} \sum_{i=1}^M \left( \hat{f}_i(\mathbf{x}) - \frac{1}{M} \sum_{i=1}^M \hat{f}_i(\mathbf{x}) \right)^2,$$

and

$$\hat{\sigma}_d^2(\mathbf{x}) = \frac{1}{M} \sum_{i=1}^M \left( \hat{f}_i(\mathbf{x}) - \hat{\hat{f}}_i(\mathbf{x}) \right)^2.$$

Assumption 3.2 tells us that

$$(f(\mathbf{x}) - \hat{f}_*(\mathbf{x}))^2 = \left( \sigma_d^2(\mathbf{x}) + \frac{\sigma_t^2(\mathbf{x})}{M} \right) \epsilon_0^2, \quad \text{with } \epsilon_0 \sim \mathcal{N}(0, 1),$$

and

$$\hat{\sigma}_t^2(\mathbf{x}) = \frac{\sigma_t^2(\mathbf{x})}{M-1} \zeta_t \quad \zeta_t \sim \chi^2(M-1).$$

Assumption 3.3 implies

$$\hat{\sigma}_d^2(\mathbf{x}) = \frac{\sigma_d^2(\mathbf{x})}{M} \zeta_d, \quad \zeta_d \sim \chi^2(M).$$

This enables us to rewrite equation (10) to

$$T^2 = \frac{\epsilon_0^2}{\gamma W_t + (1-\gamma) W_d}, \quad (11)$$

with

$$W_t = \frac{\zeta_t}{M-1}, \quad \text{and,} \quad W_d = \frac{\zeta_d}{M},$$

and

$$\gamma = \frac{\frac{\sigma_t^2(\mathbf{x})}{M}}{\sigma_d^2(\mathbf{x}) + \frac{1}{M} \sigma_t^2(\mathbf{x})},$$

where we dropped the dependence of  $\gamma$  on  $\mathbf{x}$  to simplify notation. Our goal is to bound the following probability:

$$\mathbb{P} \left( \frac{\epsilon_0^2}{\gamma W_t + (1-\gamma) W_d} > F_{1-\alpha}(1, M-1) \right), \quad (12)$$

which we can rewrite as

$$\int \int \left( \mathbb{P} \left( \frac{\epsilon_0^2}{\gamma w_t + (1-\gamma) w_d} > F_{1-\alpha}(1, M-1) \right) \right) dG_t(w_t) dG_d(w_d),$$

where  $G_t(w_t)$  is the CDF of  $W_t$  and  $G_d(w_d)$  is the CDF of  $W_d$ . We define the conditional probability in the integral as

$$\phi(\gamma) := \mathbb{P} \left( \frac{\epsilon_0^2}{\gamma w_t + (1-\gamma) w_d} > F_{1-\alpha}(1, M-1) \right). \quad (13)$$

Let  $H$  be the CDF of  $\epsilon_0^2$ , which has a  $\chi^2(1)$  distribution, then  $h = H'$  is strictly decreasing, which implies  $h' < 0$ . We can rewrite  $\phi(\gamma)$  as

$$\phi(\gamma) = 1 - H((\gamma w_t + (1-\gamma) w_d) F_{1-\alpha}(1, M-1)),$$

which gives

$$\phi'(\gamma) = -(w_t - w_d) F_{1-\alpha}(1, M-1) h((\gamma w_t + (1-\gamma) w_d) F_{1-\alpha}(1, M-1)),$$

and

$$\phi''(\gamma) = -(w_t - w_d)^2 F_{1-\alpha}(1, M-1)^2 h'((\gamma w_t + (1-\gamma) w_d) F_{1-\alpha}(1, M-1)) > 0.$$

This means that  $\phi(\gamma)$  is convex, which implies that equation (12) is convex. The maximum of equation (12) is therefore either at  $\gamma = 0$  or  $\gamma = 1$ . Evaluating equation (11) shows that taking  $\gamma = 0$  gives  $T^2$  an  $F(1, M)$  distribution and taking  $\gamma = 1$  gives  $T^2$  an  $F(1, M-1)$  distribution. Since  $F_\alpha(1, M) < F_\alpha(1, M-1)$  for all  $\alpha$ , we get

$$\mathbb{P} \left( \frac{(f(\mathbf{x}) - \hat{f}_*(\mathbf{x}))^2}{\hat{\sigma}_d^2(\mathbf{x}) + \frac{\hat{\sigma}_t^2(\mathbf{x})}{M}} > F_{1-\alpha}(1, M-1) \right) \leq \alpha. \quad \square$$

## C. Additional Experimentation

In this section we provide additional experimental results. We repeated part of Experiment 1 in Section 4 with various alterations. Firstly, we used differently distributed noise in order to see how this affects the confidence intervals. Secondly, we removed all regularisation in the neural networks. Finally, we used a different simulation model. Recall that we used a random forest that was trained on real-world data sets to be able to simulate data for our experiments. We replaced the random forest with a neural network as the true function,  $f(\mathbf{x})$ .

### C.1. Differently Distributed Noise

Here we study what would happen if we misspecified our model. In order to test this we simulated data with additive  $t(3)$  and  $\Gamma(1/10, \sqrt{10})$  distributed noise, denoted with  $\epsilon$ . In order to make the experiments comparable to the earlier ones, we used the variance  $\sigma^2(\mathbf{x})$  from the random forest and a scaling factor,  $C$ , to obtain a comparable size heteroscedastic variance:

$$y = f(\mathbf{x}) + C\sigma(\mathbf{x})\epsilon$$

For the  $t(3)$  distribution we have  $C = \sqrt{1/3}$  and for the  $\Gamma(1/10, \sqrt{10})$  distribution we have  $C = 1$ .

Table 3 illustrates that BDE still produce better confidence intervals than DE, but that the performance is affected by the violation of Assumption 3.1. In the case of the, purposely very skewed, gamma distribution, we also see that the prediction intervals are no longer calibrated, as is illustrated in Figure 7.

*Table 3.* Results of the comparison of our method Bootstrapped Deep Ensembles (BDE) to Deep Ensembles (DE) on the Concrete simulation using differently distributed additive noise. A total of 100 simulated data sets were used to calculate the metrics. Brier-CIA denotes the Brier score of the CICF of an  $A\%$  confidence interval.

NOISE	BRIER-CI90 ↓ (BDE / DE)	BRIER-CI80 ↓ (BDE / DE)	BRIER-CI70 ↓ (BDE / DE)	WIDTH CIA (BDE / DE)
$\mathcal{N}(0, 1)$	3.9E-2 / 8.4E-2	5.9E-2 / 0.11	5.9E-2 / 0.10	10.7 / 8.2
$t(3)$	4.7E-2 / 8.2E-2	6.5E-2 / 0.10	6.6E-2 / 0.10	9.8 / 8.0
$\Gamma(1/10, \sqrt{10})$	7.5E-2 / 8.7E-2	0.10 / 0.11	9.4E-2 / 0.11	8.5 / 7.0

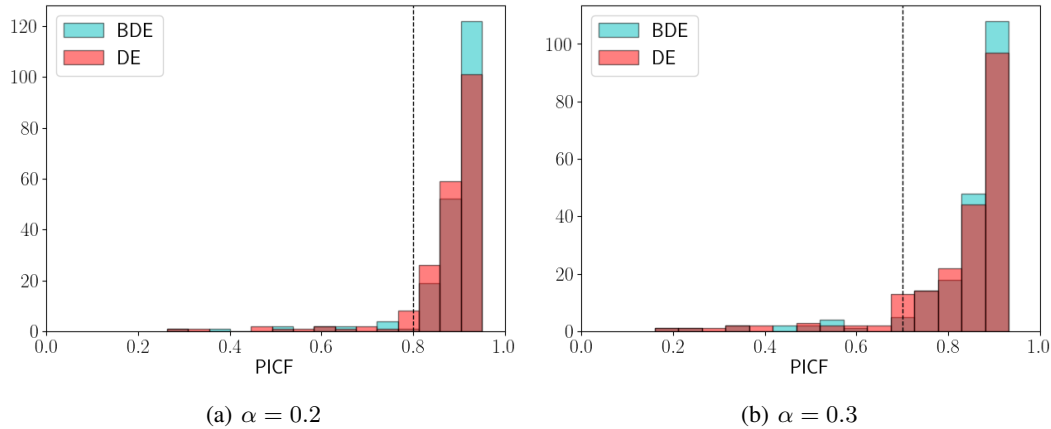


*Figure 7.* Histogram of the individual  $\text{PICF}(\mathbf{x})$  values calculated on the test set of the Concrete simulation. Each point in the histogram represents the fraction of times the true function value  $f(\mathbf{x})$  was inside the confidence interval calculated over 100 simulations. The skewness of the gamma distribution shows in the error of the PICF.

## C.2. No Regularisation

To examine the effect of regularisation we repeated a part of Experiment 1 without any regularisation. We note that the regularisation seems to have hardly any effect on the outcome. This could be the result of the fixed training time of 40 epochs and a relatively simple neural network architecture preventing overfitting.

Table 4. Results of the comparison of our method Bootstrapped Deep Ensembles (BDE) to Deep Ensembles (DE) without any regularisation. A total of 100 simulated data sets were used to calculate the metrics. On each new data set, new ensembles were trained, and new confidence and prediction intervals were constructed. Brier-CI90 denotes the Brier score of the CICF of a 90% confidence interval. Brier-PI90 denotes the equivalent quantity for the PICF. RMSE gives the root mean squared error of the predictions with respect to the targets. Since the predictor is identical for both methods, there is only one value.

SIMULATION	BRIER-CI90 ↓ (BDE / DE)	BRIER-PI90 ↓ (BDE / DE)	RMSE ↓	WIDTH PI90 (BDE / DE)	WIDTH CI90 (BDE / DE)
BOSTON	8.0E-2 / 0.11	8.9E-3 / 1.3E-2	3.82	4.32 / 3.88	11.2 / 10.7
CONCRETE	4.1E-2 / 8.6E-2	3.9E-3 / 6.8E-3	10.3	10.7 / 8.13	30.6 / 29.0
ENERGY	9.0E-2 / 0.12	6.2E-3 / 8.3E-3	2.87	2.98 / 2.43	4.98 / 4.73

## C.3. Different Simulation Method

Instead of a random forest, we used a neural network in order to simulate data (see Algorithm 4). The network has the same architecture and training procedure as the ones used for the experiment.

We see that we get better results for both BDE and DE, although BDE still perform better. A likely explanation is that this task is easier, as is indicated by the significantly lower RMSE. The model we are simulating targets from is identical to the model we are using for the experiment.

Table 5. Results of the comparison of our method Bootstrapped Deep Ensembles (BDE) to Deep Ensembles (DE) when using a neural network to simulate data. A total of 100 simulated data sets were used to calculate the metrics. On each new data set, new ensembles were trained, and new confidence and prediction intervals were constructed. Brier-CI90 denotes the Brier score of the CICF of a 90% confidence interval. Brier-PI90 denotes the equivalent quantity for the PICF. RMSE gives the root mean squared error of the predictions with respect to the targets. Since the predictor is identical for both methods, there is only one value.

SIMULATION	BRIER-CI90 ↓ (BDE / DE)	BRIER-PI90 ↓ (BDE / DE)	RMSE ↓	WIDTH CI90 (BDE / DE)	WIDTH PI90 (BDE / DE)
BOSTON	2.8E-2 / 3.1E-2	6.3E-3 / 8.8E-3	2.92	3.31 / 3.27	7.86 / 7.50
CONCRETE	2.4E-2 / 3.3E-2	4.9E-3 / 6.9E-3	6.00	7.81 / 7.12	17.7 / 16.6
ENERGY	3.7E-2 / 3.8E-2	8.5E-3 / 8.9E-3	2.64	3.10 / 1.99	5.82 / 5.53

**Algorithm 4** Pseudo-code to simulate data based on a real-world data set  $\mathcal{D}$  using a neural network.

- 1: Train a neural network on  $\mathcal{D}$  that outputs  $f(\mathbf{x})$  and  $\sigma^2(\mathbf{x})$
- 2: Simulate new targets:  $y_{\text{new}} \sim \mathcal{N}(f(\mathbf{x}), \sigma^2(\mathbf{x}))$
- 3: **Return:**  $\mathcal{D}_{\text{new}} = (X, Y_{\text{new}})$

#### C.4. Different Retraining Fractions

As expected we observe from Table 6 that the widths of the confidence intervals get larger with an increasing retraining fraction. Trivially when we setting the retraining fraction to 0 would yield zero variance and setting it to 1 would also capture the uncertainty due to random training.

Table 6. The effect of the training fraction on bootstrapped DE. A total of 100 simulated data sets were used to calculate the metrics. On each new data set, new ensembles were trained, and new confidence and prediction intervals were constructed. Brier-CI80 denotes the Brier score of the CICF of an 80% confidence interval. Brier-PI80 denotes the equivalent quantity for the PICF

RETRAINING FRACTION	BRIER-CI80 ↓ ×10 <sup>-2</sup>	BRIER-PI80 ↓ ×10 <sup>-2</sup>	WIDTH CI80	WIDTH PI80
0.1	11.5	3.0	2.84	7.37
0.2	9.1	2.6	3.16	7.54
0.3	7.8	2.5	3.4	7.64
0.4	6.1	2.1	3.7	7.89

#### C.5. RMSE values of Experiment 1

Table 7 gives the RMSE values of all methods during experiment 1 of the main text.

Table 7. The RMSE values of the methods during the simulations of experiment 1. Each value is calculated with respect to the targets of the test set and are averaged over the 100 simulations that were used for each data set. Bootstrapped Deep Ensembles and Deep Ensembles have the same score since they use they exact same predictor. Concrete Dropout has a very comparable score. The Naive Bootstrap has significantly larger errors. This is to be expected since each ensemble member is effectively being trained on less data due to the resampling.

SIMULATION	BOOTSTRAPPED DEEP ENSEMBLES	DEEP ENSEMBLES	NAIVE BOOTSTRAP	CONCRETE DROPOUT
BOSTON	3.92	3.92	4.03	3.95
CONCRETE	10.4	10.4	12.5	10.8
ENERGY	2.73	2.73	3.38	2.67
KIN8NM	0.22	0.22	0.29	0.24
NAVAL	0.013	0.013	0.018	0.013
POWER-PLANT	5.01	5.01	5.66	5.08
YACHT	3.26	3.26	3.86	2.68
WINE	0.65	0.65	0.68	0.71

### C.6. Additional Plots Experiment 1

Figures 8 and 9 give the violin plots of the CICF and PICF values from experiment 1 in the main text. These figures demonstrate that bootstrapped DE are able to provide reliable confidence and prediction intervals. Two other conclusions from the main text are also illustrated: making a prediction interval is easier and high-quality prediction intervals do not guarantee high quality confidence intervals.

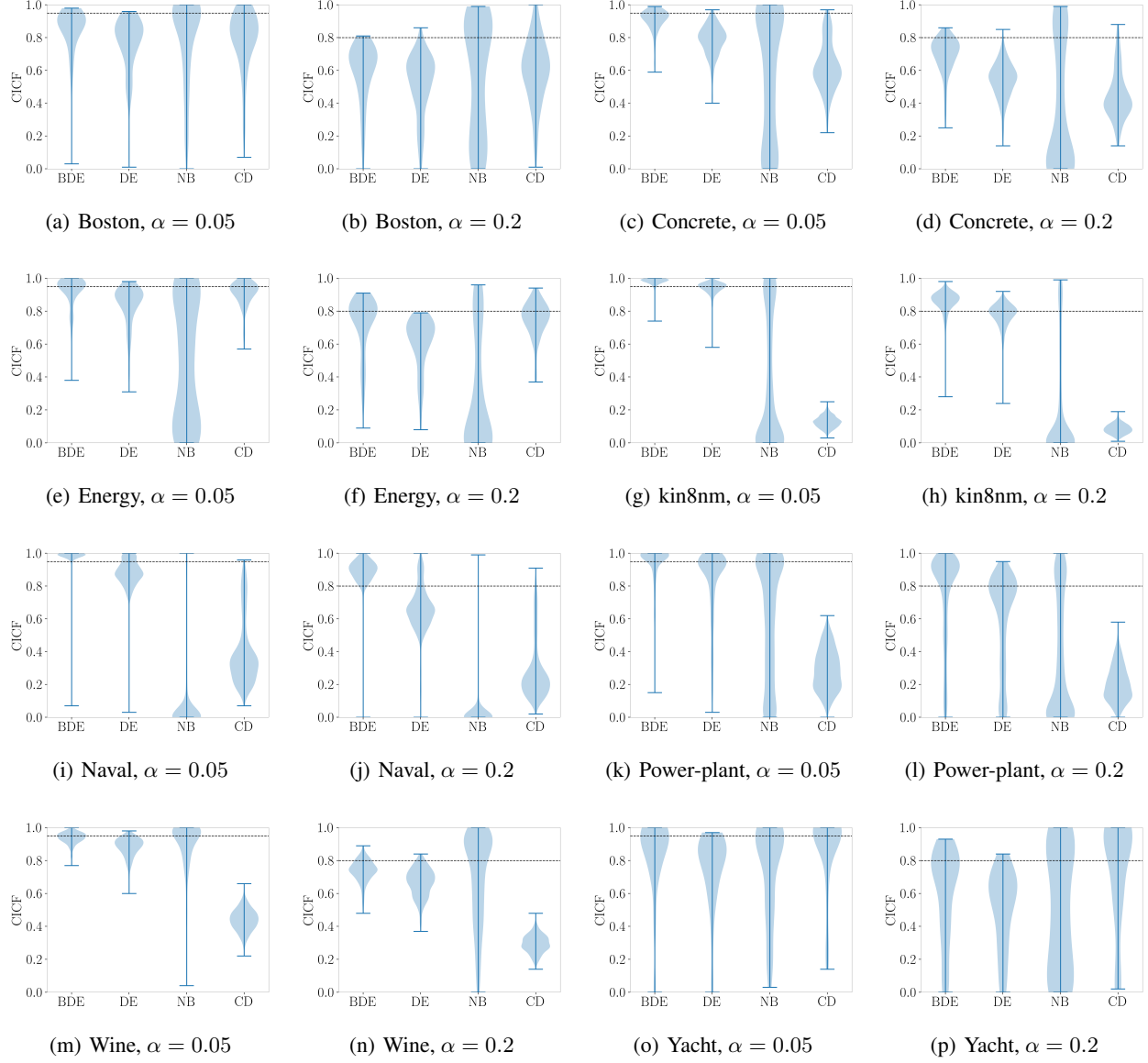


Figure 8. Violin plots of the CICF values for all 8 simulations of experiment 1 in the main text. For each simulation we give the CICF values for the 95% and 80% confidence intervals. Each plot is made using the CICF scores of each data point in the test sets. The CICF scores are calculated using 100 simulations. The confidence intervals of Bootstrapped Deep Ensembles have better coverage than the other methods in most simulations.

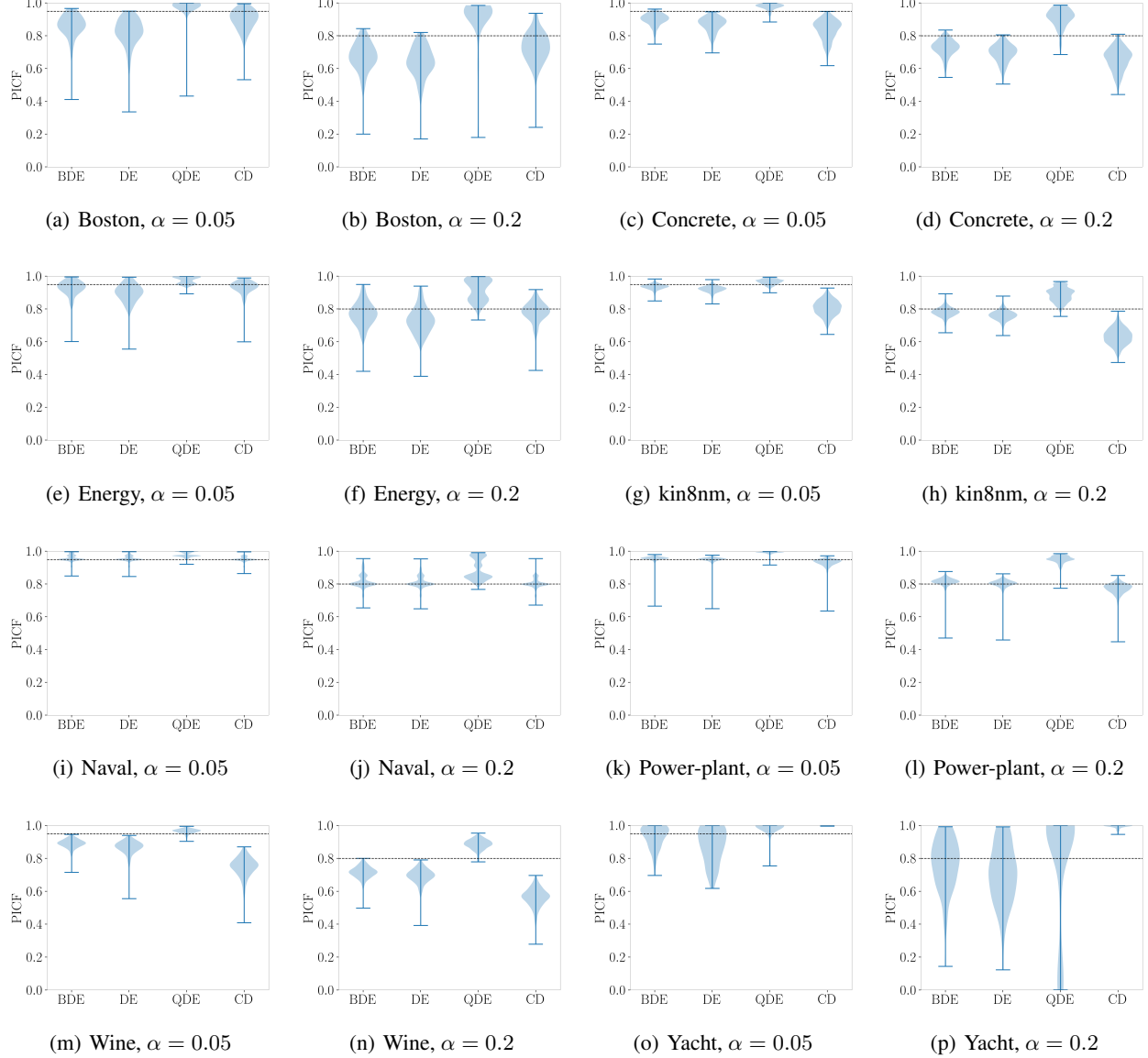


Figure 9. Violin plots of the PICF values for all 8 simulations of experiment 1 in the main text. For each simulation we give the PICF values for the 95% and 80% confidence intervals. The prediction intervals have better coverage than the confidence intervals. Quality-Driven Ensembles give prediction intervals that are too large in most simulations.